Numerical simulation of electrorheological fluids based on an extended Bingham model

Bernd Engelmann, Ralf Hiptmair, Ronald H. W. Hoppe, George Mazurkevitch

Angaben zur Veröffentlichung / Publication details:

Engelmann, Bernd, Ralf Hiptmair, Ronald H. W. Hoppe, and George Mazurkevitch. 2000. "Numerical simulation of electrorheological fluids based on an extended Bingham model." *Computing and Visualization in Science* 2 (4): 211–19. https://doi.org/10.1007/s007910050041.

Numerical simulation of electrorheological fluids based on an extended Bingham model

B. Engelmann[1], **R. Hiptmair**[2], **R.H.W. Hoppe**[3], **G. Mazurkevitch**[3]

[1] Institute of Business Management, University of Vienna, A-1090 Vienna, Austria
[2] Mathematical Institute, University of Tübingen, D-72076 Tübingen, Germany
[3] Institute of Mathematics, University of Augsburg, D-86159 Augsburg, Germany

Abstract. In the framework of the macroscopic simulation of electrorheological fluids, we present an extension of the classical Bingham model which goes beyond pure shear flows and thus enables the simulation of settings in more complex geometries. Emphasis is on the numerical solution of the resulting nonsmooth minimization problem. We propose the method of augmented Lagrangians combined with an operator-splitting technique which allows to confine the nonlinearity to local, low-dimensional problems. Numerical results are given that illustrate the electrorheological effects for various shear rates and electric field strengths in case of an electrorheological suspension rotating between two revolving cylinders.

1 Introduction

Electrorheological (ER) fluids are microstructured liquids whose rheological properties undergo a rapid change in less than a millisecond under the influence of an applied outer electric field. ER fluids usually consist of dielectric particles with mobile surface charges suspended in a non-conducting liquid. Currently, a wide variety of ER fluids is known on the basis of both silica and organic polymers (cf., e.g., [9]). In experiments, in particular for shear flows perpendicular to the applied electric field, one typically observes a viscosity increasing with the square of the field strength [9]. Moreover, at high field strengths ER fluids experience a phase transition to a viscoplastic state. It is this behavior that makes ER fluids potentially attractive for technological applications. In particular, they can be used in the automobile industry as an alternative to classical electromechanical devices to build electronically controlled clutches, motor mounts, and shock absorbers with extremely fast response times (cf., e.g., [11]).

The ER effect is due to polarization of the particles which get oriented and aligned along the direction of the electric field thus forming chains (cf., e.g., [4, 13]). Therefore, numerical simulations of ER fluids are frequently based on techniques of molecular dynamics including also other mechanisms contributing to the ER effect (see [3, 14, 16]). On the other hand, in the macroscopic regime phenomenological models in terms of continuum field equations have been used for predicting the behavior of ER fluids. Up to now, such models have been restricted to the case of pure shear flows with the Bingham fluid model as the most prominent representative (see [2, 9, 17]). Here, the shear stress σ is modeled according to

$$\sigma = g + \eta\dot{\gamma}$$

where g stands for the yield stress, η represents the viscosity and $\dot{\gamma}$ refers to the shear rate. For $\sigma < g$, the material behaves like a solid (rigid zones) whereas it undergoes a phase transition to viscous behavior as soon as σ exceeds the yield stress.

We note that for simple geometrical configurations as in Poiseuille or Couette flows the continuum field equations can be solved analytically (see, e.g., [2]). However, if the computational domain is of a more complex shape, then one has to resort to appropriate numerical solution techniques. The purpose of this paper is twofold: Firstly, in Sect. 2 we extend the classical Bingham fluid model to more general flows in terms of the minimization of the global energy dissipation. Secondly, in Sect. 3 we present the method of augmented Lagrangians as an appropriate tool for the numerical solution of that non-smooth minimization problem. Finally, Sect. 4 is devoted to a documentation of various numerical results illustrating both the ER effect in case of a simple model for an ER clutch and the viability of the model and its discretization.

2 Extension of the Bingham model

Practical ER devices rarely feature the perfect symmetry required for the pure shear flow model. Thus we need an ex-

tension of the Bingham model that covers more general geometries. We pursue a strictly phenomenological approach based on a few general principles of continuum mechanics. To obtain a sound model, nevertheless, we confine ourselves to a simple setting:

- We will only consider steady, laminar flows.
- We ignore any changes in internal energy and temperature (isothermal regime).
- We assume that viscous forces strongly dominate forces due to inertia.

Given these assumptions, the flow pattern will establish itself leading to a minimal global dissipation of energy. Hence, we have to come up with an appropriate model for the (local) rate of energy dissipation $\mathcal{D}$.

We write $\Omega \subset \mathbb{R}^3$ for the domain, in which we aim to compute the velocity field $\boldsymbol{u} := \boldsymbol{u}(\boldsymbol{x}) = (u_1(\boldsymbol{x}), u_2(\boldsymbol{x}), u_3(\boldsymbol{x}))^T$, $\boldsymbol{x} = (x_1, x_2, x_3) \in \Omega$, of the flow. The electric field $\boldsymbol{E} := \boldsymbol{E}(\boldsymbol{x})$, $\boldsymbol{x} \in \Omega$, is supposed to be known in advance. In the current setting the rate of local energy dissipation can only be a function of the rate of deformation tensor $\boldsymbol{D}(\boldsymbol{u})$, $\boldsymbol{D}(\boldsymbol{u}) := (D_{ij})_{i,j=1}^3$, $D_{ij} := \frac{1}{2}(\partial u_i/\partial x_j + \partial u_j/\partial x_i)$, $1 \le i, j \le 3$, and the electric field $\boldsymbol{E}$.

We note, that $\mathcal{D}$ must not be affected by any orthogonal coordinate transformation (*material frame indifference*) and the reversal of the direction of the flow (*time frame indifference*). Similarly, replacing $\boldsymbol{E}$ by $-\boldsymbol{E}$ should not make a difference as is suggested by empirical evidence. Following [15], we conclude that $\mathcal{D}$ has the following form

$$\mathcal{D}(\boldsymbol{u}; \boldsymbol{E}) = f(I_1, I_2, I_3, I_4, I_5, I_6) \tag{1}$$

with the invariants I_ν, $1 \le \nu \le 6$ given by

$$\begin{aligned} I_1 &:= \operatorname{tr}(\boldsymbol{E}\boldsymbol{E}^T), & I_2 &:= \operatorname{tr}(\boldsymbol{D}(\boldsymbol{u})),\\ I_3 &:= \operatorname{tr}(\boldsymbol{D}(\boldsymbol{u})^2), & I_4 &:= \operatorname{tr}(\boldsymbol{D}(\boldsymbol{u})^3),\\ I_5 &:= \operatorname{tr}(\boldsymbol{D}(\boldsymbol{u})\boldsymbol{E}\boldsymbol{E}^T), & I_6 &:= \operatorname{tr}(\boldsymbol{D}(\boldsymbol{u})^2\boldsymbol{E}\boldsymbol{E}^T) \end{aligned}$$

where tr stands for the trace of a matrix.

A reasonable assumption for most practical electrorheological fluids is that of incompressibility which allows to eliminate the dependence of the function f in (1) on I_2. Moreover, the function f is subject to the following requirements:

- For a pure shear flow, i.e., $\boldsymbol{u} = u(x_3)\boldsymbol{e}_1$, $\boldsymbol{E} = E\boldsymbol{e}_3$ ($\boldsymbol{e}_1$, $\boldsymbol{e}_3$ denote the Cartesian unit vectors in x_1- and x_3-direction.), the classical Bingham fluid model should be recovered.
- In the case of a vanishing electric field the model should yield the energy dissipation for viscous friction $\frac{1}{2}\eta\|\boldsymbol{D}(\boldsymbol{u})\|_F^2$ ($\|\cdot\|_F$ denotes the Frobenius norm of a matrix and η is the dynamic viscosity of the fluid.), which gives rise to the classical Stokes equations.
- Additional energy dissipation due to the electrorheological effect should be introduced into $\mathcal{D}$ as an extra additive term.
- The model should reflect a quadratic dependence of the yield stress on the applied electric field.

The simplest model that complies with these requirements is given by

$$\mathcal{D}(\boldsymbol{u}; \boldsymbol{E}) := \gamma|\boldsymbol{E}||\boldsymbol{D}(\boldsymbol{u})\boldsymbol{E}| + \frac{1}{2}\eta\,\|\boldsymbol{D}(\boldsymbol{u})\|_F^2\ , \tag{2}$$

where γ denotes a material-dependent constant (physical units $\mathrm{Pa\,V^{-2}}$). A comparison with the classical Bingham model in the case of pure shear flow establishes the desired relationship $g = \gamma|\boldsymbol{E}|^2$ for the yield limit in this particular case.

From a physical point of view, the first term on the right-hand side in (2) admits the interpretation as the power that is dissipated due to the snapping of particle chains, whereas the second takes into account viscous friction.

We note that the first term on the right hand side in (2) is non-differentiable. However, the rate of energy dissipation is a convex functional of $\boldsymbol{D}(\boldsymbol{u})$ so that we can formally retrieve the non-spherical part of the stress tensor $\boldsymbol{S} := \boldsymbol{S}(\boldsymbol{D}(\boldsymbol{u}), \boldsymbol{E})$ as the subgradient of $\mathcal{D}$ with respect to $\boldsymbol{D}(\boldsymbol{u})$, c.f. [7]. For the notion of the subgradient we refer, e.g., to [8]. By tedious computations, which are omitted, we get

$$\begin{aligned} \boldsymbol{S}(\boldsymbol{D}(\boldsymbol{u}), \boldsymbol{E}) = -p\boldsymbol{I} + \gamma\frac{|\boldsymbol{E}|}{2|\boldsymbol{D}(\boldsymbol{u})\boldsymbol{E}|}\left(\boldsymbol{D}(\boldsymbol{u})\boldsymbol{E}\boldsymbol{E}^T + \boldsymbol{E}\boldsymbol{E}^T\boldsymbol{D}(\boldsymbol{u})\right)\\ + \eta\boldsymbol{D}(\boldsymbol{u})\ , \end{aligned} \tag{3}$$

once $\boldsymbol{D}(\boldsymbol{u})\boldsymbol{E} \neq 0$. Obviously the stress tensor is not well defined where $\boldsymbol{D}(\boldsymbol{u})\boldsymbol{E} = 0$, which characterizes the "*rigid zones*" in this model. Yet, the term is slightly misleading, since now a gliding of the particle chains is possible. For instance, for a constant electric field in $\boldsymbol{e}_3$ direction the velocity $\boldsymbol{u}$ in the rigid zones has to meet the constraints $\frac{\partial u_3}{\partial x_3} = 0$, $\frac{\partial u_2}{\partial x_3} + \frac{\partial u_3}{\partial x_2} = 0$, $\frac{\partial u_1}{\partial x_3} + \frac{\partial u_3}{\partial x_1} = 0$. These are satisfied for velocity fields of the form $\boldsymbol{u} = (u_1(x_1, x_2), u_2(x_1, x_2), 0)^T$, for example.

Remark 1. From (3) we can derive the estimate $\|\boldsymbol{S} + p\boldsymbol{I}\|_F \ge \gamma|\boldsymbol{E}|^2$, i.e. the shear stress has to exceed the threshold $\gamma|\boldsymbol{E}|^2$ outside rigid zones. Thus, $\gamma|\boldsymbol{E}|^2$ turns out to be a proper equivalent of the *yield limit* of the standard Bingham model.

Based on the model (2) for the local energy dissipation the velocity field $\boldsymbol{u}$ can be computed as the solution of the following nonsmooth minimization problem for the global rate of energy dissipation:
Find $\boldsymbol{u} \in \boldsymbol{V}$ such that

$$J_{ER}(\boldsymbol{u}) = \inf_{\boldsymbol{v}\in\boldsymbol{V}} J_{ER}(\boldsymbol{v})\ , \tag{4}$$

where

$$J_{ER}(\boldsymbol{v}) := \gamma\int_\Omega |\boldsymbol{E}||\boldsymbol{D}(\boldsymbol{v})\boldsymbol{E}|\,d\boldsymbol{x} + \frac{1}{2}\eta\int_\Omega \|\boldsymbol{D}(\boldsymbol{v})\|_F^2\,d\boldsymbol{x} - l(\boldsymbol{v})\ . \tag{5}$$

Here $\boldsymbol{V} := \{\boldsymbol{v} \in H^1(\Omega)^3,\ \operatorname{div}\boldsymbol{v} = 0,\ \boldsymbol{v}_{|\Gamma_D} = 0\}$, where $H^1(\Omega)$ stands for the Sobolev space of square integrable functions with square integrable generalized first derivatives (cf., e.g., [1]) and Γ_D denotes that part of the boundary $\Gamma = \partial\Omega$ where no-slip boundary conditions are prescribed. The functional $l : \boldsymbol{V} \mapsto \mathbb{R}$ takes into account boundary and volume forces and is of the form [12, Ch. 5]

$$l(\boldsymbol{v}) = \int_\Omega \langle \boldsymbol{f}, \boldsymbol{v}\rangle\,d\boldsymbol{x} + \int_{\Gamma_F} \langle \boldsymbol{f}_s, \boldsymbol{v}\rangle\,d\sigma + \int_{\Gamma_P} f_p\,\langle \boldsymbol{v}, \boldsymbol{n}\rangle\,d\sigma\ . \tag{6}$$

Here, $\boldsymbol{f}$ stands for a field of volume forces, Γ_F is that part of the boundary, where the surface force $\boldsymbol{f}_s$ is prescribed. On Γ_P we impose the pressure f_p.

3 The method of augmented Lagrangians

We consider the numerical solution of the nonsmooth minimization problem (4) in the case of a geometrical configuration which may be thought of as a simple model for an electrorheological clutch (cf., e.g., [11]): The gap between two open conducting cylinders is filled with an electrorheological fluid (see Fig. 1). When the outer cylinder starts revolving, the inner, which is supposed to be at rest, experiences a torque due to the viscosity of the fluid. Applying a voltage through an external electric circuit, the electrorheological effect leads to enhanced viscosity and the strength of the torque felt by the inner cylinder will rise.

The arrangement has full rotational symmetry. This carries over to the electric field, which, in cylindrical coordinates, can be represented as

$$\boldsymbol{E}(r,z,\phi) = E_r(r,z)\boldsymbol{e}_r + E_z(r,z)\boldsymbol{e}_z$$

where $\boldsymbol{e}_r$ and $\boldsymbol{e}_z$ are the coordinate vectors in radial and axial direction, respectively. For a velocity distribution $\boldsymbol{u}$ that solves (4) we can thus conclude that it can only feature a tangential component: $\boldsymbol{u} = \boldsymbol{u}(r,z) = u(r,z)\boldsymbol{e}_\varphi$. Please note, that a priori such velocity fields are divergence free.

In the current symmetric setting, the global energy dissipation reads as follows

$$J_{ER}(u) = \pi\gamma \int_\Omega |\boldsymbol{E}||\boldsymbol{E}\cdot\nabla u| r\, d(r,z) + \frac{1}{2}\pi\eta \int_\Omega |\nabla u|^2 r\, d(r,z) \tag{7}$$

where the two-dimensional computational domain Ω corresponds to the longitudinal section of the three-dimensional physical domain with the r,z-plane. We impose zero boundary values for u along the axis and the walls of the inner cylinder. At the walls of the outer cylinder the boundary values for u are determined by the speed of the rotation.

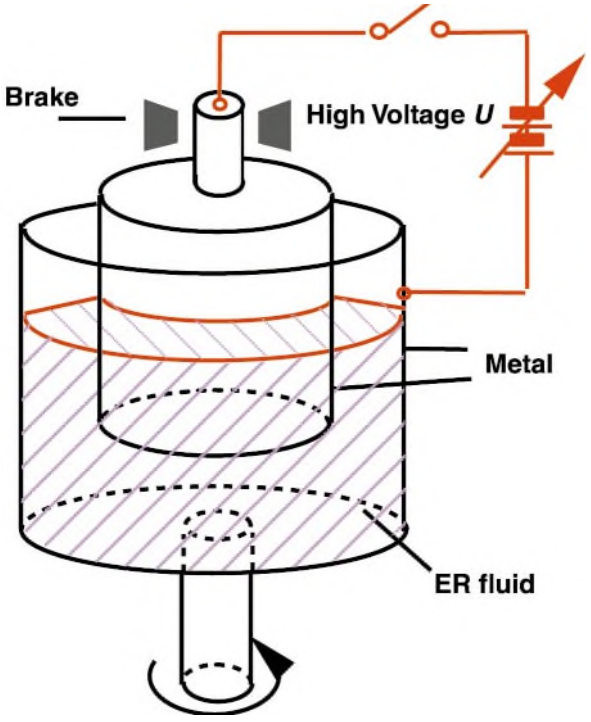

Fig. 1. Model for an electrorheological clutch

The method of augmented Lagrangians (cf., e.g., [10]) relies on an equivalent formulation of the minimization problem as a saddle point problem by introducing ∇u as an additional unknown $\boldsymbol{p}$ and by coupling the constraint $\boldsymbol{p} = \nabla u$ by means of both a Lagrangian multiplier $\boldsymbol{\mu}$ and a penalty term. Combined with an appropriate operator-splitting technique, this method allows to confine the nonlinearity to local problems of small dimension.

We set $V \subset H^1(\Omega)$ for the space of all eligible velocity components satisfying the boundary conditions and define the Lagrangian $L^\tau_{ER} : V \times L_2(\Omega)^2 \times L_2(\Omega)^2 \to \mathbb{R}$ according to

$$\begin{aligned} L^\tau_{ER}(u,\boldsymbol{p},\boldsymbol{\mu}) := {} & \pi\gamma \int_\Omega |\boldsymbol{E}||\boldsymbol{E}\cdot\boldsymbol{p}| r\, d(r,z) \\ & + \frac{1}{2}\pi\eta \int_\Omega |\boldsymbol{p}|^2 r\, d(r,z) \\ & + \int_\Omega \boldsymbol{\mu}\cdot(\boldsymbol{p}-\nabla u)\, d(r,z) \\ & + \frac{1}{2}\tau \int_\Omega |\boldsymbol{p}-\nabla u|^2\, d(r,z)\,, \end{aligned} \tag{8}$$

where $\tau > 0$ stands for the penalty parameter. Then, the saddle point problem is given by:

Find $(u,\boldsymbol{p},\boldsymbol{\lambda}) \in V \times L^2(\Omega)^2 \times L^2(\Omega)^2$ such that

$$L^\tau_{ER}(u,\boldsymbol{p},\boldsymbol{\mu}) \le L^\tau_{ER}(u,\boldsymbol{p},\boldsymbol{\lambda}) \le L^\tau_{ER}(v,\boldsymbol{q},\boldsymbol{\lambda})$$

for all $(v,\boldsymbol{q},\boldsymbol{\mu}) \in V \times L^2(\Omega)^2 \times L^2(\Omega)^2$, or equivalently

$$L^\tau_{ER}(u,\boldsymbol{p},\boldsymbol{\lambda}) = \inf_{(v,\boldsymbol{q})\in V\times L^2(\Omega)^2} \sup_{\boldsymbol{\mu}\in L^2(\Omega)^2} L^\tau_{ER}(v,\boldsymbol{q},\boldsymbol{\mu})\,. \tag{9}$$

For the discretization of the saddle point problem (9) we use a finite element approximation with respect to a simplicial triangulation $\mathcal{T}_h$ of the computational domain Ω. In particular, we approximate V by the finite element space $V_h := S_1(\Omega;\mathcal{T}_h) := \{v_h \in C(\bar\Omega),\ v_{h|T} \in P_1(T),\ T \in \mathcal{T}_h\}$ of continuous, piecewise linear finite elements (see [6]). On the other hand, for the approximation of the dual variable $\boldsymbol{p} \in L^2(\Omega)^2$ and the Lagrangian multiplier $\boldsymbol{\lambda} \in L^2(\Omega)^2$ we can resort to the space $\boldsymbol{W}_h$ of, w.r.t. $\mathcal{T}_h$, piecewise constant, discontinuous vectorfields.

Likewise, in (8) the supplied electric field $\boldsymbol{E}$ is approximated by $\boldsymbol{E}_h \in \boldsymbol{W}_h$ where, for instance, we may choose $\boldsymbol{E}_{h|T}$, $T \in \mathcal{T}_h$, as the value $\boldsymbol{E}(C)$ of $\boldsymbol{E}$ in the center of gravity of $T \in \mathcal{T}_h$. Normally, if $\boldsymbol{E}$ is obtained from another finite element computation on the same mesh $\mathcal{T}_h$, it will only be available as a locally constant function.

In the end, we are led to the following discrete saddle point problem:

Find $(u_h,\boldsymbol{p}_h,\boldsymbol{\lambda}_h) \in V_h \times \boldsymbol{W}_h \times \boldsymbol{W}_h$ such that

$$L^\tau_{ER}(u_h,\boldsymbol{p}_h,\boldsymbol{\mu}_h) \le L^\tau_{ER}(u_h,\boldsymbol{p}_h,\boldsymbol{\lambda}_h) \le L^\tau_{ER}(v_h,\boldsymbol{q}_h,\boldsymbol{\lambda}_h)$$

for all $(v_h, \boldsymbol{q}_h, \boldsymbol{\mu}_h) \in V_h \times \boldsymbol{W}_h \times \boldsymbol{W}_h$, or, equivalently,

$$L^{\tau}_{ER}(u_h, \boldsymbol{p}_h, \boldsymbol{\lambda}_h) = \inf_{(v_h, \boldsymbol{q}_h) \in V_h \times \boldsymbol{W}_h} \sup_{\boldsymbol{\mu}_h \in \boldsymbol{W}_h} L^{\tau}_{ER}(v_h, \boldsymbol{q}_h, \boldsymbol{\mu}_h) \, . \tag{10}$$

Note that (10) satisfies the Ladyzhenskaja–Babuška–Brezzi (LBB-) condition which ensures the well-posedness of the discrete saddle point problem (cf., e.g., [5]).

We solve (10) iteratively by means of an operator splitting method where each iteration step amounts to the successive solution of a global linear minimization problem and local, i.e., elementwise nonlinear minimization problems including appropriate updates of the discrete Lagrangian multipliers.

In particular, given startiterates $(\boldsymbol{p}_h^0, \boldsymbol{\lambda}_h^1) \in \boldsymbol{W}_h \times \boldsymbol{W}_h$ and sequences $(\tau_n)_{n\in\mathbb{N}}$, $(\rho_n)_{n\in\mathbb{N}}$ of penalization parameters $\tau_n > 0$ and update parameters $\rho_n > 0$, $n \in \mathbb{N}$, an iteration involves the following two steps:

1st step: Find $u_h^n \in V_h$ such that

$$L^{\tau_n}_{ER}\left(u_h^n, \boldsymbol{p}_h^{n-1}, \boldsymbol{\lambda}_h^n\right) = \inf_{v_h \in V_h} L^{\tau_n}_{ER}\left(v_h^n, \boldsymbol{p}_h^{n-1}, \boldsymbol{\lambda}_h^n\right) \tag{11}$$

and compute $\boldsymbol{\lambda}_h^{n+\frac{1}{2}} \in \boldsymbol{W}_h$ according to

$$\boldsymbol{\lambda}_h^{n+\frac{1}{2}} = \boldsymbol{\lambda}_h^n + \rho_n \left(\nabla u_h^n - \boldsymbol{p}_h^{n-1}\right) \, . \tag{12}$$

2nd step: Find $\boldsymbol{p}_h^n \in \boldsymbol{W}_h$ such that

$$L^{\tau_n}_{ER}\left(u_h^n, \boldsymbol{p}_h^n, \boldsymbol{\lambda}_h^{n+\frac{1}{2}}\right) = \inf_{\boldsymbol{q}_h \in \boldsymbol{W}_h} L^{\tau_n}_{ER}\left(u_h^n, \boldsymbol{q}_h, \boldsymbol{\lambda}_h^{n+\frac{1}{2}}\right) \tag{13}$$

and compute $\boldsymbol{\lambda}_h^{n+1} \in \boldsymbol{W}_h$ by means of

$$\boldsymbol{\lambda}_h^{n+1} = \boldsymbol{\lambda}_h^{n+\frac{1}{2}} + \rho_n \left(\nabla u_h^n - \boldsymbol{p}_h^n\right) \, . \tag{14}$$

We note that the necessary and sufficient optimality condition for the global minimization problem (11) of the first step is given by the variational equation:

Find $u_h^n \in V_h$ such that

$$\int_\Omega \nabla u_h^n \cdot \nabla v_h \, d(r,z) = \tau_n^{-1} \int_\Omega \boldsymbol{\lambda}_h^n \cdot \nabla v_h d(r,z) + \int_\Omega \boldsymbol{p}_h^{n-1} \cdot \nabla v_h d(r,z), \quad v_h \in V_h \, . \tag{15}$$

The computation of $u_h^n \in V_h$ requires the solution of a linear algebraic system where the coefficient matrix corresponds to the stiffness matrix associated with the continuous, piecewise linear finite element approximation of the Laplacian $-\Delta$.

On the other hand, due to the definition of $\boldsymbol{W}_h$ the minimization problem (13) of the second step reduces to the simultaneous solution of the elementwise minimization problems:

For each $T \in \mathcal{T}_h$ find $\boldsymbol{p}_{h|T}^n \in P_0(T)^2$ such that

$$J_T^{\tau_n}(\boldsymbol{p}_{h|T}^n) = \inf_{\boldsymbol{q}_h^T \in P_0(T)^2} J_T^{\tau_n}(\boldsymbol{q}_h^T),$$

$$J_T^{\tau_n}(\boldsymbol{q}_h^T) := J^{\tau_n}_{ER}\left(u_{h|T}^n, \boldsymbol{q}_h^T, \boldsymbol{\lambda}_h^{n+\frac{1}{2}}\right) \, . \tag{16}$$

We write $\boldsymbol{E}_C$ for the constant value of the electric field on T and set for the solution of (16)

$$\boldsymbol{p}_{h|T}^n := \alpha_1 \boldsymbol{E}_C + \alpha_2 \boldsymbol{E}_C^{\perp} \, , \quad T \in \mathcal{T}_h \, ,$$

where $\boldsymbol{E}_C^{\perp}$ is an arbitrarily, but fixed vector perpendicular to $\boldsymbol{E}_C$. Then, the coefficients α_i, $1 \le i \le 2$, can be easily obtained by the solution of two separate quadratic minimization problems. Indeed, setting

$$a := \pi\eta \int_T |\boldsymbol{E}_C|^2 r \, d(r,z) + \tau_n \int_T |\boldsymbol{E}_C|^2 \, d(r,z) \, ,$$

$$b := \tau_n \int_T \nabla u_h^n \cdot \boldsymbol{E}_C \, d(r,z) - \int_T \boldsymbol{\lambda}_h^{n+\frac{1}{2}} \cdot \boldsymbol{E}_C \, d(r,z) \, ,$$

$$c := \pi\gamma \int_T |\boldsymbol{E}_C|^3 r \, d(r,z) \, ,$$

and defining $a^{\perp}$ and $b^{\perp}$ in the same way with $\boldsymbol{E}_C$ replaced by $\boldsymbol{E}_C^{\perp}$, we obtain

$$\alpha_1 = \begin{cases} (b+c)/a & \text{if} \quad b < -c \\ (b-c)/a & \text{if} \quad b > c \\ 0 & \text{if} \quad -c \le b \le c \end{cases} \, , \quad \alpha_2 = \frac{b^{\perp}}{a^{\perp}} \, .$$

4 Numerical results

We have applied the method of augmented Lagrangians to the case of a rotating electrorheological fluid between two revolving coaxial cylinders as described in the previous section (cf. Fig. 1).One of the cylinders rotates with a constant angular speed ω, while the other one is supposed to be at rest.

We are interested in computing both the distribution of the angular velocity $u(r,z)\boldsymbol{e}_{\varphi}$ of the fluid in the gap between both cylinders and the overall torque. To compute the torque we rely on the principle of conservation of energy: All the power dissipated in the fluid must be supplied by the rotation of

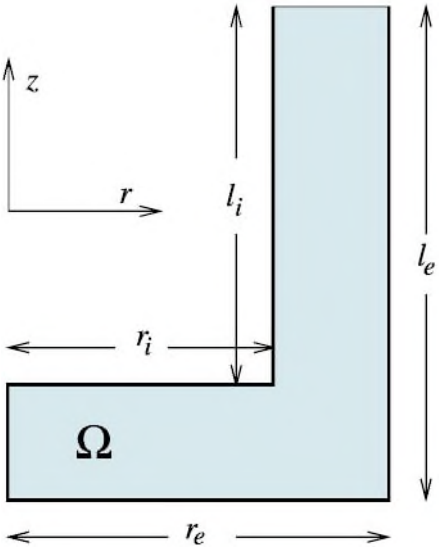

Fig. 2. Computational domain for clutch simulation

the driven cylinder. Thus the angular momentum transferred through the clutch amounts to $N = J_{ER}(\boldsymbol{u})/\omega$, where J_{ER} is the functional from (5). The value of this functional can be readily computed from the finite element solution u_h.

As far as the material data are concerned, we have considered an electrorheological suspension with dynamic viscosity $\eta = 0.90 \times 10^{-1}\,\mathrm{kg\,m^{-1}s^{-1}}$ and $\gamma = 1 \times 10^{-9}\,\mathrm{NV^{-2}}$ (cf. [2, Sect. I]). A voltage U between the two cylinders was prescribed and the electric field $\boldsymbol{E}$ was approximately computed by solving the boundary value problem for the electrostatic potential

$$\begin{aligned} -\operatorname{div}\epsilon\nabla\Psi &= 0 \quad \text{in } \Omega \\ u &= 0 \quad \text{on the walls of the outer cylinder} \\ u &= U \quad \text{on the walls of the inner cylinder} \\ \tfrac{\partial u}{\partial \boldsymbol{n}} &= 0 \quad \text{elsewhere on } \partial\Omega\,, \end{aligned} \tag{17}$$

Rotational symmetry renders the potential constant in angular direction and hence, we can assume $\Psi = \Psi(r, z)$. The resulting two-dimensional problem is equivalent to the variational equation:
Find $\Psi \in H^1_\Gamma(\Omega) + \Psi_0$ such that

$$\int_\Omega r\,\langle \nabla\Psi, \nabla v\rangle\; d(r,z) = 0\,, \quad \forall v \in H^1_\Gamma(\Omega)\,,$$

where $H^1_\Gamma(\Omega)$ contains the functions of $H^1(\Omega)$ with zero trace on the inner and outer cylinder and Ψ_0 is some potential that complies with the Dirichlet boundary conditions from (17). The variational problem is discretized by means of standard piecewise continuous finite elements on $\mathcal{T}_h$. Then, $\boldsymbol{E}$ can be obtained as the elementwise constant gradient of the finite element solution for Ψ.

To enhance the resolution of the finite element method, we employ adaptive grid refinement. The refinement process is controlled by a simple error indicator that triggers the refinement of elements where large gradients of u_h occur. Thus we can save significant computational resources compared with finite element schemes on uniform grids.

A meaningful termination criterion for the augmented Lagrangian iteration depends on the objective of the calculation. We implemented two options: First, when one is interested in some global (integral) characteristics of the system (torque, energy) it is reasonable to monitor the decrease of the total dissipated energy $J_{ER}(u_h)$: Due to (8), the Lagrangian $L^\tau_{ER}(u, \boldsymbol{p}, \boldsymbol{\mu})$ has the representation:

$$L^\tau_{ER}(u, \boldsymbol{p}, \boldsymbol{\mu}) = J_{ER}(u) + L_{AU}(u, \boldsymbol{p}, \boldsymbol{\mu})\,,$$

with

$$\begin{aligned} L_{AU}(u, \boldsymbol{p}, \boldsymbol{\mu}) = &\int_\Omega \boldsymbol{\mu}\cdot(\boldsymbol{p} - \nabla u)\, d(r,z) \\ &+ \frac{1}{2}\tau \int_\Omega |\boldsymbol{p} - \nabla u|^2\, d(r,z)\,. \end{aligned}$$

For heuristic reasons we assume that the iterates are close to the stationary point once we have

$$\frac{|\,L_{AU}(u^n)\,|}{J_{ER}(u^n)} < tol\,, \tag{18}$$

for a small threshold *tol*.

On the other hand the criterion (18) may not be sufficient to resolve local features of u, for instance, large gradients. In this case it makes sense to require

$$\|\boldsymbol{p} - \nabla u\|_{L^2} < tol\,. \tag{19}$$

Before we present the results of numerical simulations for pure shear mode (Couette flow) and a more complicated flow structure in case of an electrorheological clutch, let us comment on the observed convergence behavior of the augmented Lagrangian approach. The numerical experiments revealed a mesh independent convergence, i.e., the convergence rates do not depend on the granularity of the triangulations. On the other hand, in accordance with the findings in [10], we did observe a dependence on the choice of the penalty parameter τ. In particular, we found that there exists a threshold value τ^* such that for $\tau \geq \tau^*$ we have monotone convergence whereas for $\tau < \tau^*$ the convergence shows an oscillatory behavior. Moreover, this value τ^* depends on the the strength of the applied electric field $\boldsymbol{E}$ in the sense that it increases with increasing field strength.

Couette flow

The first suite of numerical experiments studies Couette flow, i.e., $l := l_i = l_e$ and natural boundary conditions are imposed on the top and the bottom of the gap between the cylinders. Consequently, we end up with an inherently one-dimensional setting, where only radial dependence remains: $\boldsymbol{u} = u(r)\boldsymbol{e}_\phi$. This is also true for the electric field, which reads

$$\boldsymbol{E} = \boldsymbol{E}(r) = \frac{U}{\ln(r_e/r_i)}\frac{1}{r}\,\boldsymbol{e}_r\,.$$

The simplified energy dissipation functional (7) now runs

$$\begin{aligned} J_{ER}(u) = \pi\gamma l \left(\frac{U}{\ln(r_e/r_i)}\right)^2 &\int_{r_i}^{r_e} \frac{1}{r}\left|\frac{\partial u}{\partial r}\right|\, dr \\ &+ \frac{1}{2}\pi\eta l \int_{r_i}^{r_e} \left|\frac{\partial u}{\partial r}\right|^2 r\, dr\,. \end{aligned} \tag{20}$$

In this particular setting, the problem can even be solved analytically: Any function minimizing (20) has to be monotone so that we can assume $u'(r) := \frac{\partial u}{\partial r} \geq 0$. In a flow zone $I \subset]r_i, r_e[$, where $u' > 0$, we can derive the following variational problem:
Find $u \in H^1_0(I)$, u fixed at the endpoints of I, such that

$$c_0 \int_I \frac{v'}{r}\, dr - c_1 \int_I r u' v'\, dr = 0\,, \quad \forall v \in H^1_0(I)\,.$$

Here $c_0 := \pi\gamma l \left(\frac{U}{\ln(r_e/r_i)}\right)^2$ and $c_1 := \pi\eta l$. This yields the Euler equation

$$c_1\left(r u'\right)' - c_0\frac{1}{r^2} = 0\,. \tag{21}$$

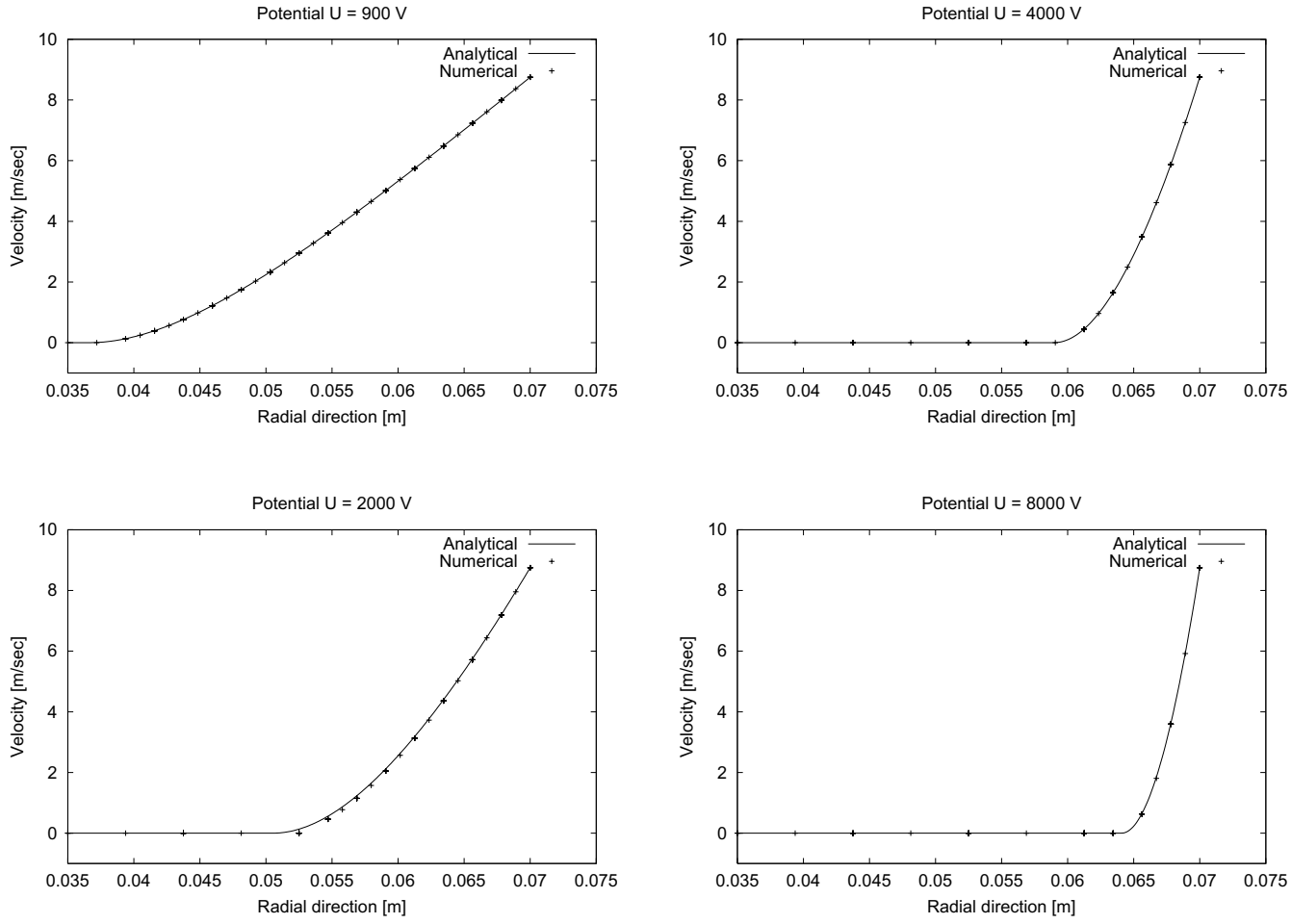

Fig. 3. Angular velocity profiles for different values of applied potential U

Now assume that there is one plug zone $]r_i, x[$, $r_i \le x < r_e$, sticking to the inner cylinder, which is at rest. This is suggested by numerical evidence. Solving (21) with boundary values $u(x) = 0$ and $u(r_e) = r_e\omega$ we get the profile for angular velocity

$$u(r) = \begin{cases} 0 & \text{for } r_i \le r \le x \\ \dfrac{c_0}{c_1}\dfrac{1}{r} + A(x)\ln r + B(x) & \text{for } x \le r \le r_e \end{cases}, \tag{22}$$

with parameters $A(x)$ and $B(x)$ defined by

$$\begin{aligned} A &= \frac{1}{\ln\dfrac{r_e}{x}}\left(r_e\omega + \frac{c_0}{c_1}\left(\frac{1}{x} - \frac{1}{r_e}\right)\right) \\ B &= -\frac{1}{\ln\dfrac{r_e}{x}}\left(r_e\omega\ln x + \frac{c_0}{c_1}\left(\frac{\ln r_e}{x} - \frac{\ln x}{r_e}\right)\right). \end{aligned} \tag{23}$$

The end of the plug zone x as a function of input parameters $x = x(U, \gamma, \omega, r_i, r_e)$ is defined from the condition $u'(x) = 0$, which yields the the following equation to determine x:

$$-\frac{c_0}{c_1}\frac{1}{x} + A(x) = 0 \iff \ln\frac{r_e}{x}\frac{c_0}{c_1} = xr_e\omega + \frac{c_0}{c_1}\left(1 - \frac{x}{r_e}\right). \tag{24}$$

An exact solution of the nonlinear problem (24) can be easily computed. We point out that the solution of (22)–(24) is different from the analytical solution computed in [2], because in the current model inertia has been neglected. From (20) and (22) we determine the total rate of energy dissipation as a function of the applied voltage and the angular speed ω of the outer cylinder:

$$E_{\text{diss}} = E_{\text{diss}}(U, \gamma, \omega, r_i, r_e) = J_{ER}(u; U, \gamma, \omega, r_i, r_e). \tag{25}$$

Finally, we obtain the torque

$$\begin{aligned} N &:= N(U, \omega, r_i, r_e) = E_{\text{diss}}(U, \gamma, \omega, r_i, r_e)/\omega \\ &= \frac{\mathcal{N}(r_e) - \mathcal{N}(x)}{\omega}, \end{aligned} \tag{26}$$

with

$$\mathcal{N}(r) = \frac{c_1}{2}A^2\ln r + \frac{1}{4r^2}\frac{c_0^2}{c_1}.$$

We computed the Couette flow in a fully two-dimensional fashion, also employing a finite element approximation of the electrostatic potential. The plots in Fig. 3 show the analytical versus the computed values for the angular velocity as a function of r. Here we used $l = 70\,\text{cm}$, $r_i = 3.5\,\text{cm}$, $r_e = 7\,\text{cm}$, $\omega = 125\,\text{rad}\,\text{s}^{-1}$, $\eta = 0.90 \times 10^{-1}\,\text{kg}\,\text{m}^{-1}\text{s}^{-1}$ and $\gamma = 1 \times 10^{-9}\,\text{NV}^{-2}$.

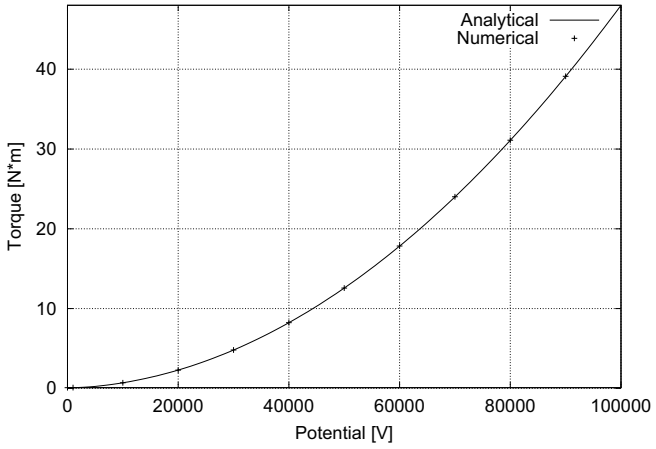

Fig. 4. Torque N as a function of applied potential U (solid line = analytic solution, points = torque obtained from finite element computations)

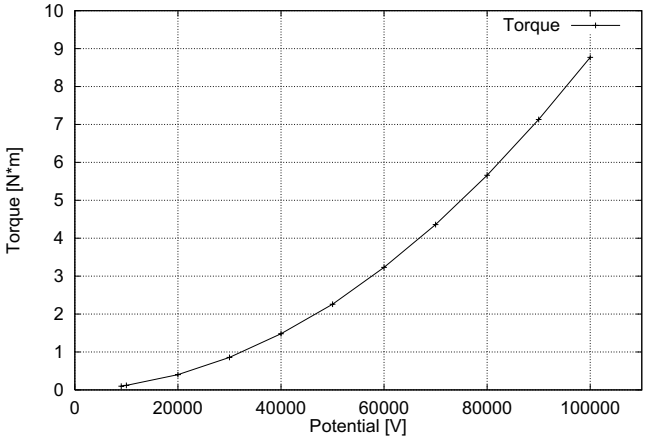

Fig. 5. Wide gap: Torque N as a function of applied voltage U

Table 1. Discretization errors for selected test potentials U

Number of elements	Velocity $\|u_h - u\|_{H^1}$		Torque $\|N_h - N\|$	
	$U = 2 \times 10^4$	$U = 8 \times 10^4$	$U = 2 \times 10^4$	$U = 8 \times 10^4$
166	1.37	15.2	4.7×10^{-3}	6.1×10^{-1}
664	0.71	9.0	1.2×10^{-3}	1.9×10^{-1}
2656	0.34	5.3	3.2×10^{-4}	4.7×10^{-2}
10624	0.16	2.7	8.1×10^{-5}	1.3×10^{-2}

For the same geometry, Fig. 4 shows the analytical and computed torque as a function of the applied voltage U.

The approximation properties of the finite element scheme and the discretization errors on regularly refined grids for the velocity and the torque are given in Table 1. Here, u_h and N_h denote the finite element solutions whereas u and N refer to

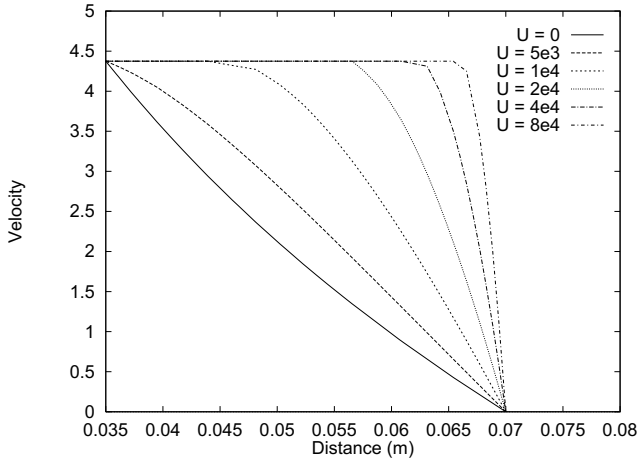

Fig. 6. Wide gap: Angular veclocity profiles for different values of potential U (in V)

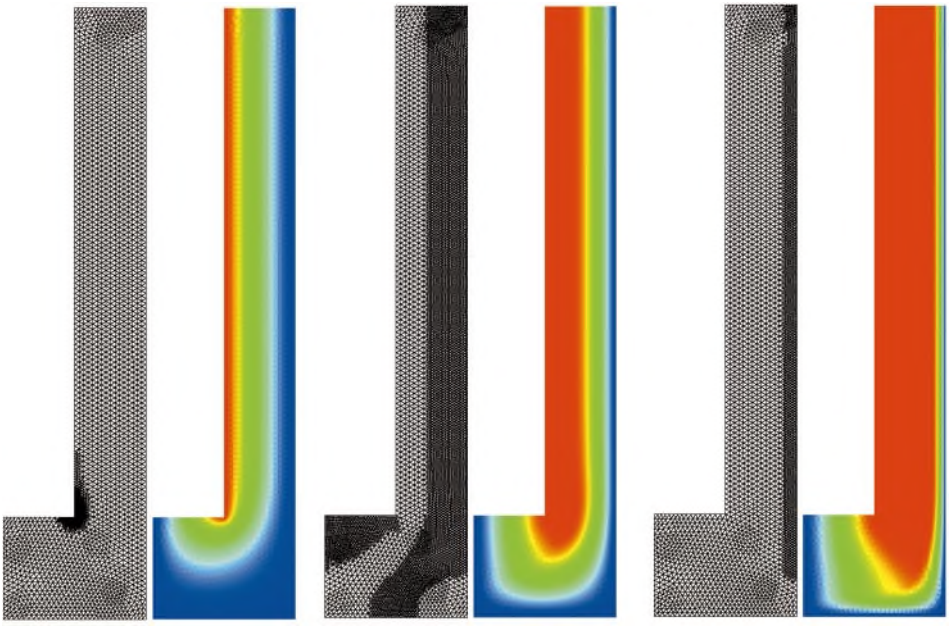

Fig. 7. Wide gap: Computational grids and velocity distribution for $U = 0$ V (*left*), $U = 1 \times 10^4$ V (*middle*) and $U = 4 \times 10^4$ V (*right*)

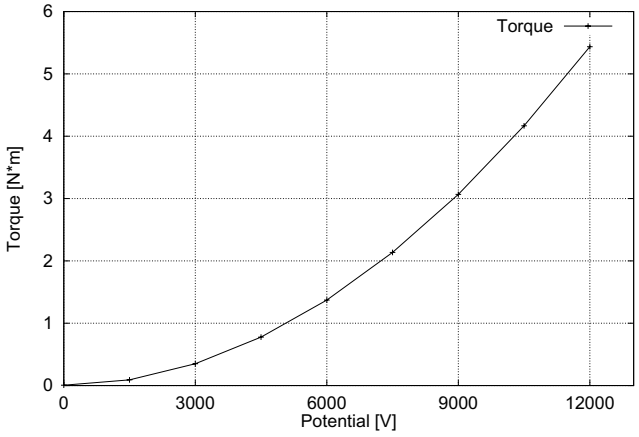

Fig. 8. Torque N as a function of applied voltage U (in V)

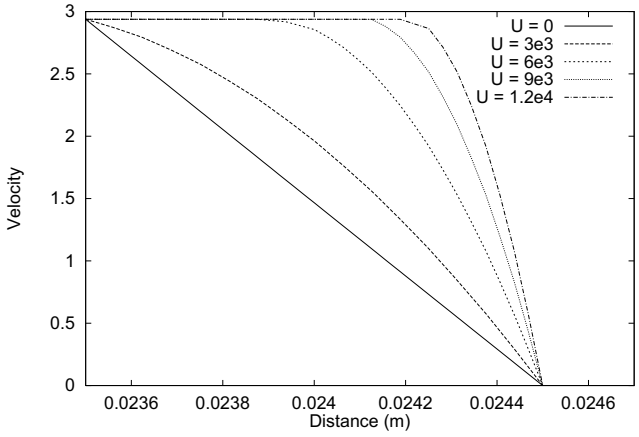

Fig. 9. Narrow gap: Angular veclocity profiles for different values of potential U

the analytical ones as given by (22)–(24) and (26) respectively. Since most of the error is localized in the the drag zone, $x < r < r_e$, where the gradients of the velocity can be extremely high, local refinement is strongly recommended in order to obtain reliable results with minimal computational costs.

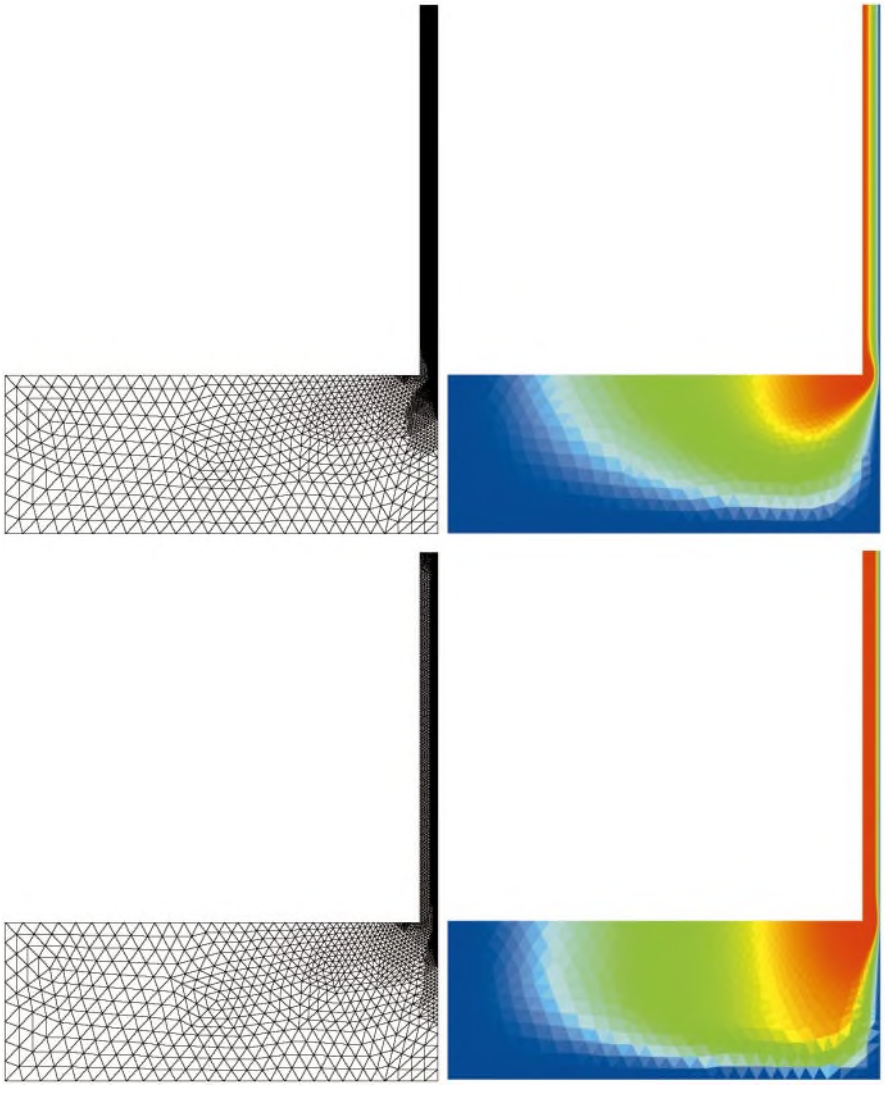

Fig. 10. Narrow gap: Computational grids and velocity distribution for $U = 3 \times 10^3$ V (*top*) and $U = 9 \times 10^3$ V (*bottom*)

Electrorheological clutch

Wide Gap. We have chosen a geometrical configuration with the radii $r_i = 3.5$ cm, $r_e = 7$ cm and heights $\ell_i = 25$ cm, $\ell_e = 30$ cm (see Fig. 2). For our computations we fixed the angular velocity at $\omega = 125\,\mathrm{rad\,s^{-1}}$ on the inner cylinder. We carried out the simulation for a wide range of values for the applied voltage U. In Fig. 5 the resulting torques are plotted versus U. In Fig. 6 the computed velocity profiles are depicted for different voltages. Figure 7 shows examples of computational grids and velocity equipotentials. There, for the sake of visuability, only one level of adaptive refinement is shown.

Narrow Gap. A second series of experiments uses the same fluid but a different geometry: $r_i = 23.5$ mm, $r_e = 24.5$ mm, $\ell_i = 21.0$ mm, $\ell_e = 30.0$ mm. For $\omega = 125\,\mathrm{rad\,s^{-1}}$ we carried out the same computations as above. Figures 8–10 show the results of numerical computations for this case.

Acknowledgements. The authors have been supported by the German National Science Foundation (DFG) within the Sonderforschungsbereich 438 (Mathematical Modeling, Simulation, and Verification of Material-Oriented Processes and Intelligent Systems).

References

1. Adams, R.: Sobolev Spaces. New York: Academic Press 1975
2. Atkin, R., Shi, X., Bullough, W.: Solution of the constitutive equations for the flow of an electrorheological fluid. J. Rheol. 35: 1441–1461 (1991)
3. Bonnecaze, R., Brady, J.: Dynamic simulation of an electrorheological fluid. J. Chem. Phys. 96: 2183–2202 (1992)
4. Bonnecaze, R., Brady, J.: Yield stresses in electrorheological fluids. J. Rheol. 38: 73–115 (1992)
5. Brezzi, F., Fortin, M.: Mixed and hybrid finite element methods. New York: Springer 1991
6. Ciarlet, P.: The finite element method for elliptic problems, Amsterdam: North-Holland 1978
7. Duvaut, G., Lions, J.: Inequalities in Mechanics and Physics. Berlin, Heidelberg, New York: Springer 1976
8. Ekeland, I., Temam, T.: Convex Analysis and Variational Problems. Amsterdam: North-Holland 1976
9. Filisko, F.: Overview of ER technology. In: Progress in ER technology. Havelka, K. (Ed.) New York: Plenum Press 1995
10. Glowinski, R., LeTallec, P.: Augmented Lagrangian and Operator-Splitting Methods in Nonlinear Mechanics. Vol. 9 of SIAM Studies in Applied Mathematics. Philadelphia: SIAM 1989
11. Hartsock, D., Novak, R. Chaundy, G.: ER fluid requirements for automotive devices. J. Rheol. 35: 1305–1326 (1991)
12. Ionescu, R., Sofonea, M.: Functional and Numerical Methods in Viscoplasticity. Oxford: Oxford University Press 1993
13. Mokeev, A., Korobko, E., Vedernikova, L:, Structural viscosity of electrorheological fluids. J. Non-Newtonian Fluid Mech. 42: 213–230 (1992)
14. Parthasarathy, M., Klingenberg, D.: A microstructural investigation of the nonlinear response of electrorheological suspensions. Rheol. Acta 34: 417–429 (1995)
15. Rajagopal, K., Wineman, A.: Flow of electrorheological materials. Acta Mechanica 91: 57–75 (1992)
16. Whittle, M.: Computer simulation of an electrorheological fluid. J. Non-Newtonian Fluid Mech. 37: 233–263 (1990)
17. Whittle, M, Atkin, R.J., Bullough, W.: Fluid dynamic limitations on the performance of an electrorheological clutch. J. Non-Newtonian Fluid Mech. 57: 61–81 (1995)